Supporting Information

Rational Design of Flexible Capacitive Sensors with Highly Linear Response over a Broad Pressure Sensing Range

Jianing Wu,[#a] Yagang Yao,[#b] Yuhan Zhang,[a] Tianyu Shao,[a] Hao Wu,[c] Shaoyu Liu,[c] Zhuo Li,*[a] and Limin Wu*[a]

[a] Department of Materials Science and State Key Laboratory of Molecular Engineering of Polymers, Fudan University, Shanghai, 200433, China

E-mail: lmw@fudan.edu.cn , zhuo_li@fudan.edu.cn

[b] National Laboratory of Solid State Microstructures, College of Engineering and Applied Sciences, Jiangsu Key Laboratory of Artificial Functional Materials and Collaborative Innovation Center of Advanced Microstructures, Nanjing University, Nanjing 210093, China

[c] State Key Laboratory of Digital Manufacturing Equipment and Technology, School of Mechanical Science and Engineering, Huazhong University of Science and Technology, Wuhan, 430074, China

[#] Equal contribution to this work.

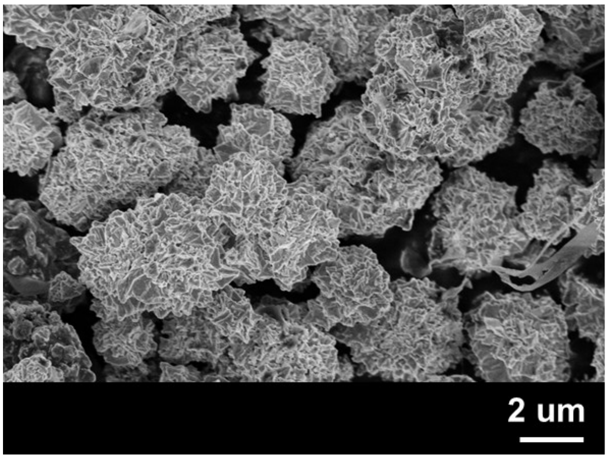

Fig. S1 The SEM image of spiky Ni particles.

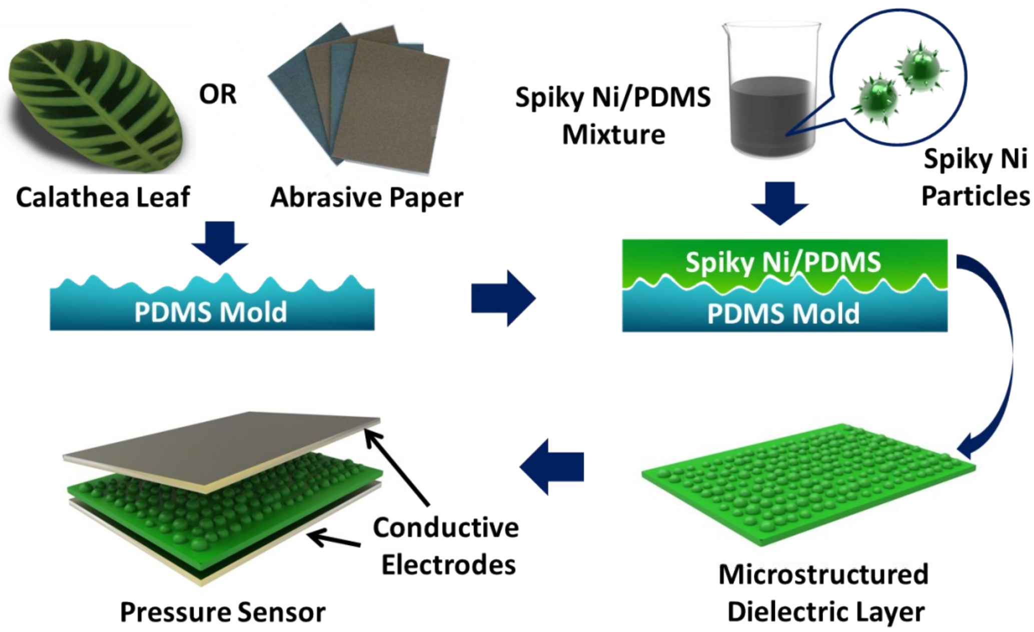

Fig. S2 Fabrication of the dielectric layer with microstructure prepared from calathea zebrine leaf or abrasive paper.

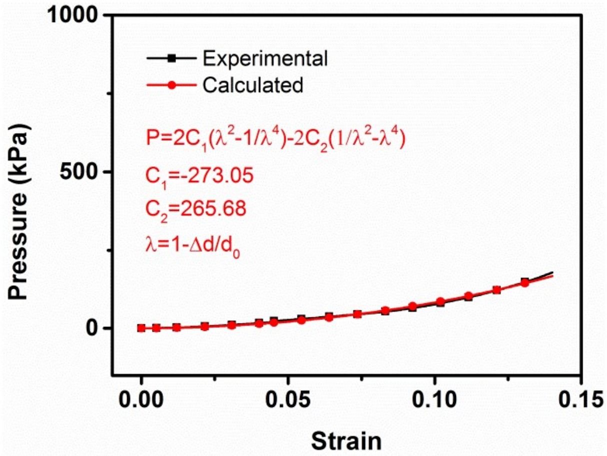

Fig. S3 Experimental and calculated compression stress (pressure)-strain (thickness change) curves of the 29.0 vol% spiky Ni/PDMS composite.

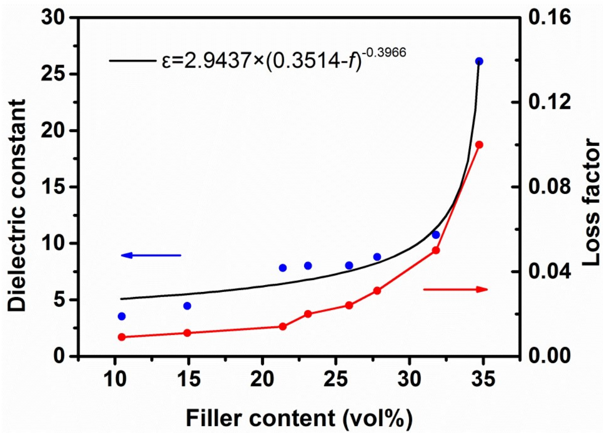

Fig. S4 Dielectric constant (blue) and loss factor (red) of spiky Ni/PDMS composites as function of filler volume percentage. The black curve is a fitting curve of percolation theory.

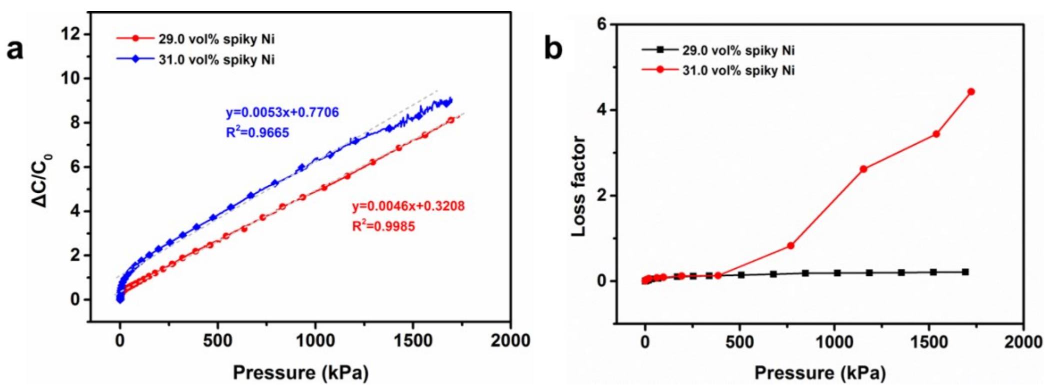

Fig. S5 (a) The actual change of capacitance as a function of the applied pressure. (b) The loss factor as a function of applied pressure.

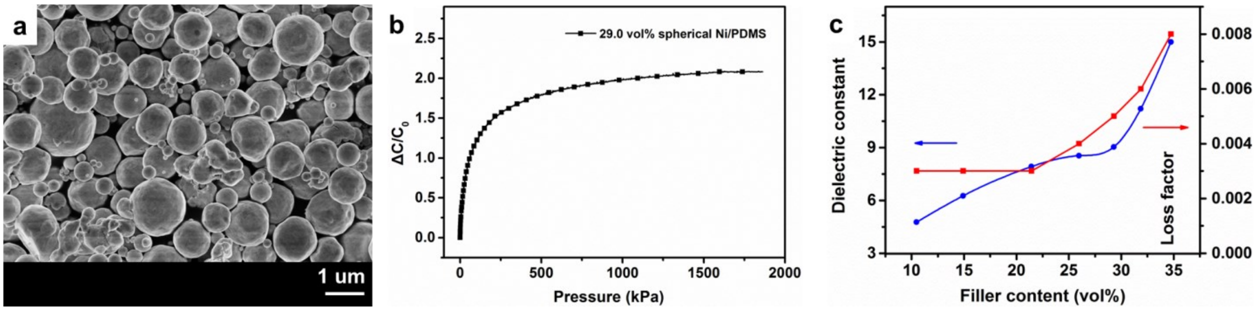

Fig. S6 (a) The SEM images of spherical Ni particles. (b) The change of capacitance as a function of the applied pressure. (c) The percolation curve of the spherical Ni/PDMS dielectric layer.

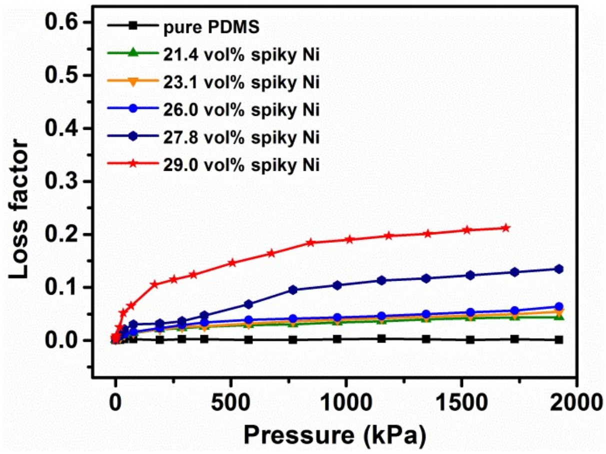

Fig. S7 The loss factor as a function of applied pressure, including data from the composites with 21.4 vol.%, 23.1 vol.%, 26 vol.%, 27.8 vol.%, 29.0 vol.% spiky Ni and pure PDMS.

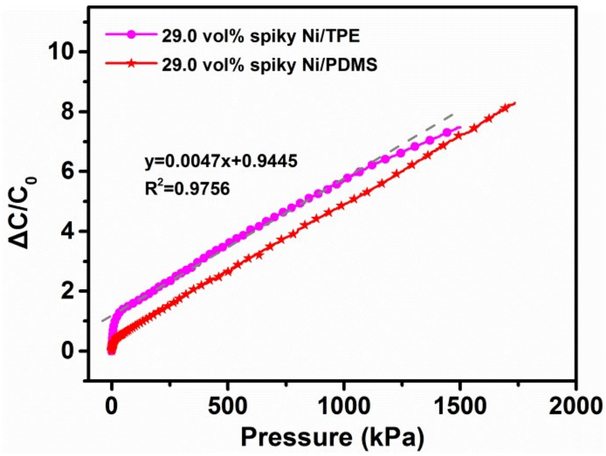

Fig. S8 The change of capacitance as a function of the applied pressure, and the linear fitting of the sensitivity curves of two different composites.

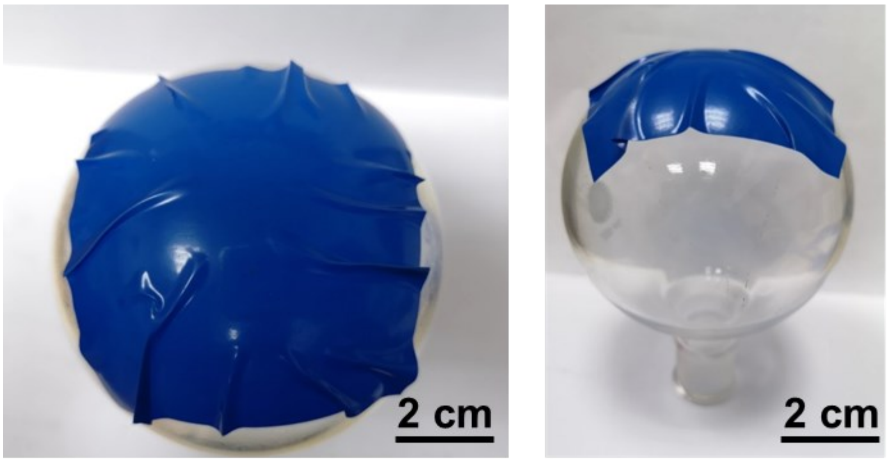

Fig. S9 Digital photos of the traditional flexible film covering at the bottom of the flask.

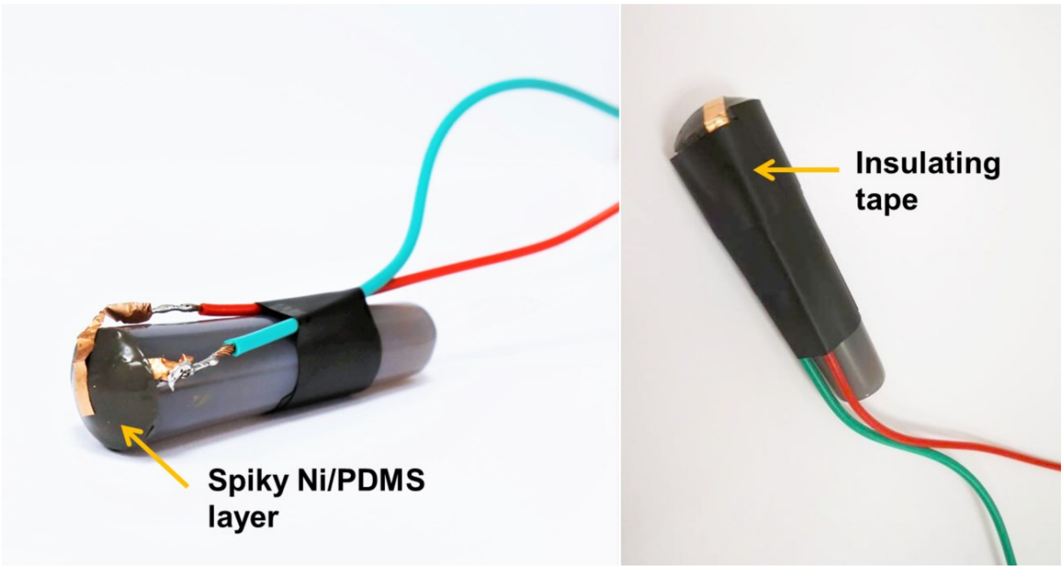

Fig. S10 Digital photos of the sensor covering at curved surface.

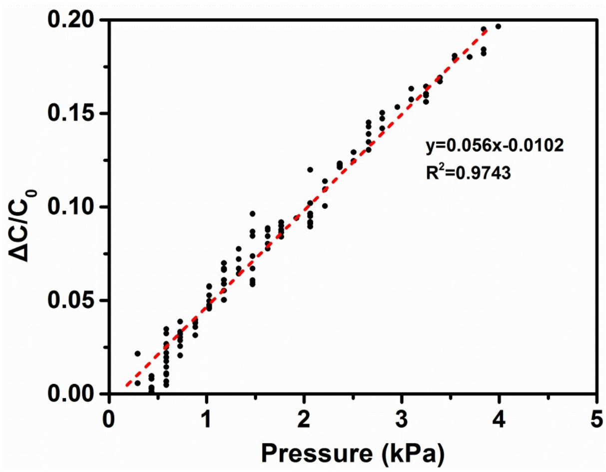

Fig. S11 The change of capacitance as a function of the applied pressure at lower than 4 kPa. Since the air pressure changes 1.2 kPa when the altitude increases by 100 meters, the equvalent capacitance change is approximately 0.0672. That is, the linear coefficient between altitude and capacitance change is 100/0.0672=1488.

Table S1. The characterization of the dielectric layer composites (calculated).

Sample	Fitted Curve
21.4 vol% spiky Ni	y=0.0018x+0.0374, R^2=0.9633
23.1 vol% spiky Ni	y=0.002x+0.0401, R^2=0.9680
26.0 vol% spiky Ni	y=0.0028x+0.0452, R^2=0.9804
27.8 vol% spiky Ni	y=0.004x+0.0456, R^2=0.9918
29.0 vol% spiky Ni	y=0.0058x+0.0337, R^2=0.9951
31.0 vol% spiky Ni	y=0.0085x+0.0264, R^2=0.9844

Table S2. The characterization of the dielectric layer composites (experimental).

Sample	Fitted Curve
pure PDMS	y=0.0002x+0.1741, R^2=0.7622
21.4 vol% spiky Ni	y=0.0007x+0.3529, R^2=0.8706
23.1 vol% spiky Ni	y=0.0009x+0.4572, R^2=0.8600
26.0 vol% spiky Ni	y=0.001x+0.5094, R^2=0.8499
27.8 vol% spiky Ni	y=0.0022x+0.3753, R^2=0.9857
29.0 vol% spiky Ni	y=0.0046x+0.3208, R^2=0.9985
31.0 vol% spiky Ni	y=0.0053x+0.7706, R^2=0.9665

Table S3. Typical sensitivities, working ranges and linearity of previously reported linear flexible capacitive pressure sensors.

Materials	Sensitivity (kPa^{-1})	Detection range (kPa)	S×LMR	Linearity	Journal	Ref
our work-flat surface	0.0046	0-1700	7.8	0.999	-	-
our work-with leaf surface structure	0.0216	0-500	10.8	0.9978	-	-
our work-with abrasive paper surface structure	1.149	0-20	23.0	0.9989	-	-
silver nanowires/PDMS	0.00016	0-500	0.08	-	Nanoscale	[1]
carbon black/silicone rubber	0.0002536	0-700	1.65	0.9981	Meas. Sci. Technol.	[2]
PDMS/CIP with a hair-like micro cilia array structure	0.28	0-10	2.8	0.981	J. Mater. Chem. A	[3]
microstructural single-walled carbon nanotubes/PDMS	0.7	0-25	17.5	-	Adv. Mater.	[4]
porous carbon black/PDMS	1.1	0-10	11.0	-	Nanotechnology	[5]

Table S4. Typical sensitivities and working ranges of recently capacitive pressure sensors

Materials	Sensitivity (kPa^{-1})	Detection range (kPa)	Journal	Ref
PDMS dielectric layer with hollow micro-pillars	0.0014 (10-20 kPa) 0.0005 (20-120 kPa)	10-120	Nano Energy	[6]
MXene/PVDF-TrFE composite nanofibrous scaffolds as a dielectric layer between PEDOT:PSS electrodes	0.51 (0-1 kPa) 0.011 (10-150 kPa) 0.006 (150-400 kPa)	0-400	ACS Appl. Mater. Inter.	[7]
PDMS pyramids	0.55	0-7	Nat. Mater.	[8]
polyurethane/multiwalled carbon nanotubes	0.753 (< 2 kPa) 0.0549 (2-50 kPa)	0.1-50	ACS Appl. Mater. Inter.	[9]
PDMS film with uniformly distributed micro-pores as a dielectric layer	1.18	0-0.02	Sensor. Actuat. A-Phys.	[10]
AgNWs/PDMS as the electrode, while PVDF as the dielectric layer	2.94 (0-1.5 kPa) 0.75 (1.5-7 kPa)	0-7	ACS Appl. Mater. Inter.	[11]
AgNWs/PDMS as the electrode, while PVP or PMMA as the dielectric layer	3.8 (0.045-0.5 kPa) 0.8 (0.5-2 kPa) 0.35 (2-5 kPa)	0.045-5	Nanoscale	[12]
porous film loading with ionic liquid on the fabric skeleton, then coated with AgNWs	4.46 (< 0.5 kPa); 0.5 (0.5-10 kPa) 0.0143 (10-120 kPa)	0-120	Mater. Today Phys.	[13]
PVDF-TrFE interlocked microstructure	6.583 (0-0.1 kPa) 0.125 (0.1-0.9 kPa)	0-0.9	Small	[14]
PDMS pyramids and Polyisoindigobithiophene-siloxane transistor	8.4 (0-8 kPa) 0.38 (8-60 kPa)	0-60	Nat. Commun.	[15]

Video S1. The response of the sensor during it descends and ascends in water at certain speed**.**

References

1 S. S. Yao and Y. Zhu, *Nanoscale*, 2014, **6**, 2345-2352.

2 X. H. Guo, Y. Huang, X. Cai, C. X. Liu and P. Liu, *Meas. Sci. Technol.*, 2016, **27**, 045105.

3 Q. Zhou, B. Ji, Y. Z. Wei, B. Hu, Y. B. Gao, Q. S. Xu, J. Zhou and B. P. Zhou, *J. Mater. Chem. A*, 2019, **7**, 27334.

4 G. Y. Bae, J. T. Han, G. Lee, S. Lee, S. W. Kim, S. Park, J. Kwon, S. Jung and K. Cho, *Adv. Mater.*, 2018, **30**, 1803388.

5 P. Q. Wei, X. L. Guo, X. B. Qiu and D. L. Yu, *Nanotechnology*, 2019, **30**, 455501.

6 C. Zhang, S. Y. Liu, X. Huang, W. Guo, Y. Y. Li and H. Wu, *Nano Energy*, 2019, **62**, 164-170.

7 S. Sharma, A. Chhetry, M. Sharifuzzaman, H. Yoon and J. Y. Park, *ACS Appl. Mater. Inter.*, 2020, **12**, 22212-22224.

8 S. C. B. Mannsfeld, B. C. K. Tee, R. M. Stoltenberg, C. V. H. H. Chen, S. Barman, B. V. O. Muir, A. N. Sokolov, C. Reese and Z. Bao, *Nat. Mater.*, 2010, **9**, 859-864.

9 Z. Y. Gao, Z. Lou, W. Han and G. Z. Shen, *ACS Appl. Mater. Inter.*, 2020, **12**, 24339-24347.

10 B. Y. Lee, J. Kim, H. Kim, C. Kim and S. D. Lee, *Sensor. Actuat. A-Phys.*, 2016, **240**, 103-109.

11 X. Shuai, P. Zhu, W. Zeng, Y. Hu, X. Liang, Y. Zhang, R. Sun and C. P. Wong, *ACS Appl. Mater. Inter.*, 2017, **9**, 26314-26324.

12 Y. Joo, J. Byun, N. Seong, J. Ha, H. Kim, S. Kim, T. Kim, H. Im, D. Kim and Y. Hong, *Nanoscale*, 2015, **7**, 6208-6215.

13 J. Yang, Q. Liu, Z. Deng, M. Gong, F. Lei, J. Zhang, X. Zhang, Q. Wang, Y. Liu, Z. Wu and C. F. Guo, *Mater. Today Phys.*, 2019, **8**, 78-85.

14 H. S. Niu, S. Gao, W. J. Yue, Y. Li, W. J. Zhou and H. Liu, *Small*, 2020, **16**, 1904774.

15 G. Schwartz, C. K. Tee, J. Mei, A. L. Appleton, D. H. Kim, H. Wang and Z. Bao, *Nat. Commun.*, 2013, **4**, 1859.